INSTITUTE OF PHYSICS PUBLISHING NANOTECHNOLOGY
Nanotechnology **16** (2005) 2039–2043 doi:10.1088/0957-4484/16/10/009

Fabrication, characterization and field emission properties of large-scale uniform ZnO nanotube arrays

Xiao-Ping Shen[1], Ai-Hua Yuan[2], Ye-Min Hu[3], Yuan Jiang[1], Zheng Xu[1,4] and Zheng Hu[3]

[1] State Key Laboratory of Coordination Chemistry, Nanjing University, Nanjing 210093, People's Republic of China
[2] School of Materials Science and Engineering, Jiangsu University of Science and Technology, Zhenjiang 212003, People's Republic of China
[3] Laboratory of Mesoscopic Materials Science, Department of Chemistry, Nanjing University, Nanjing 210093, People's Republic of China

E-mail: zhengxu@netra.nju.edu.cn

Received 9 May 2005, in final form 5 July 2005
Published 3 August 2005
Online at stacks.iop.org/Nano/16/2039

Abstract
Large-scale well-aligned ZnO nanotubes with outer diameters of 100–300 nm and lengths of tens of micrometres have been prepared by a template-based chemical vapour deposition method. The photoluminescence spectrum of the ZnO nanotube arrays consists of a strong violet band at 414 nm, a blue band at 462 nm and a weak shoulder peak at around 480 nm. The field emission of the ZnO nanotube arrays shows a turn-on field of about 7.3 V μm^{-1} at a current density of 0.1 $\mu A\ cm^{-2}$ and emission current density up to 1.3 mA cm^{-2} at a bias field of 11.8 V μm^{-1}.

1. Introduction

In recent years, one-dimensional (1D) nanostructures have stimulated considerable interest for scientific research due to their importance in mesoscopic physics and their potential applications in nanotechnology. The development of nanodevices might benefit from the distinct morphology and high aspect ratio of nanotubes and nanowires. In particular, nanotubes possess several different areas of contact (borders, inner and outer surfaces, and structured tube walls) that in principle can be functionalized in several ways such as the incorporation of nanorods in nanotubes and more generally used as nanoscale host materials. Moreover, the tubular nanostructures might exhibit some interesting physical and chemical properties unattainable by other nanostructures, and open up possibilities for various new application fields such as catalysis, intramolecular junctions, storage and release systems. Therefore, the explorations of new fabrication methods for nanotubes have become an active subject. Up to now, many kinds of nanotubes, such as sulfides, nitrides, and oxides, have been reported [1, 2]. Zinc oxide, a wide band-gap (3.37 eV) semiconductor with high exciton binding energy (60 meV), has a wide range of applications in solar cells [3], sensors [4], optoelectronic devices, and surface acoustic waveguides [5]. With good thermal and chemical stability, 1D ZnO nanostructures are potential candidates for field emitters with long lifetimes. Recently, various 1D ZnO nanostructures, including nanowires [6–11], nanorods [12–14], and nanobelts [15], have been extensively studied and field emission from ZnO nanowires [8–11], nanorods [14] and nanoneedles [16–18] have been explored. However, the study on nanotubular ZnO is quite limited [19–22], and field emission from ZnO nanotubes has not been reported so far. In this study, well-aligned ZnO nanotube arrays were fabricated via a simple template-based chemical vapour deposition (CVD) method, and field electron emission from ZnO nanotube arrays was investigated.

2. Experimental details

Reagent grade zinc acetylacetonate hydrate [$Zn(CH_3COCHCOCH_3)_2 \cdot H_2O$] was used as the CVD precursor without further purification. Commercially available porous anodic

[4] Author to whom any correspondence should be addressed.

alumina (PAA) membranes (Whatman Ltd, Anodisc 13) with a nominal pore diameter of 100 nm and thickness of 60 μm (actual pore diameter of about 100–300 nm) were used as templates. The apparatus used for synthesis of ZnO nanotubes is a conventional tube furnace with a horizontal quartz tube. In a typical experiment, the organometallic precursor (∼300 mg) in a ceramic boat was placed at the upstream end and the PAA template was placed vertically at the central high-temperature zone of the tube furnace. O_2 was used as both a carrier and a reactive gas for both the oxide synthesis and the removal of organic ligands as oxidized volatile byproducts. After the system had been evacuated to 100 Pa, O_2 was kept flowing through the quartz tube from the precursor to the template. The gas flow rate was 30 sccm (standard cubic centimetres per minute) and the pressure of the system was maintained at about 1.5 kPa. The furnace was then heated to 500 °C at a rate of 10 °C min^{-1} and kept at this temperature for 1 h for CVD. The precursor was situated in advance according to the temperature gradient from the centre to the ends of the tube furnace so that its temperature could be held at about 200 °C. After deposition, the pumping was stopped and air was admitted into the reactor. The temperature of the furnace was raised to 600 °C at a rate of 5 °C min^{-1} and maintained for 4 h for annealing. The resulting template was collected after the furnace was cooled to room temperature. The cover layer on the surface of the resulting template was removed by polishing with 1500 grid sandpaper for further characterization and detection.

The as-deposited products with PAA membranes support were characterized with a D/Max-RA x-ray diffractometer with Cu Kα radiation. The morphology and the composition of the products were examined by scanning electron microscopy (SEM, JSM-840A) equipped with an energy dispersive spectrometry (EDS). The structure and diffraction pattern of the nanotubes were investigated by transmission electron microscopy (TEM, JEM-200CX). Photoluminescence (PL) studies were conducted using a Aminco Bowman Series 2 fluorescence spectrophotometer with an Xe lamp at room temperature. The excitation wavelength was 302 nm. The field emission measurements were carried out by a two parallel-plate configuration in a vacuum chamber with a pressure of 1.6×10^{-4} Pa. The distance between the electrodes was 200 μm. The dependence of the emission current on the applied voltage was recorded automatically by a field emission detection system.

Specimens for SEM were prepared as follows. The sample was fixed at a piece of copper tape and immersed in 1 mol l^{-1} NaOH aqueous solution for about 1 h to remove the alumina template. After careful rinsing with deionized water and drying, the tape was attached to an SEM sample stub and was sputtered with a thin layer of gold. Samples for TEM were prepared by placing a piece of the resulting membrane in 2 mol l^{-1} NaOH aqueous solution for about 40 min to dissolve the alumina. The solution was removed carefully using a syringe and the sample was rinsed with distilled water at least twice. The sample was collected on a carbon-coated copper grid and allowed to air-dry before measurement. Specimens for field emission measurement was prepared as follows. An Au thin film was deposited on one side of the resulting membrane in order to reduce the influence of PAA membrane on conductance, and 2 mol l^{-1} NaOH aqueous solution was dropped onto the other side of the resulting membrane to partially dissolve the alumina for about 10 min. After careful rinsing with deionized water and drying, the membrane with its sputtered Au side was attached to a stainless-steel plate using conducting glue as cathode for field emission measurement.

3. Results and discussion

Figure 1 shows SEM images and an EDS spectrum of the as-prepared ZnO nanotubes. Figure 1(a) shows a low-magnification SEM image of aligned ZnO nanotubes after partly removing PAA templates. The surface layer was not completely removed, which made the ZnO nanotubes stick together. The lengths of the nanotubes are up to several tens of micrometres. From figure 1(b), it can be seen that the nanotubes have open ends and are arranged in a parallel and well-ordered way. The diameters of the nanotubes are in the range 100–300 nm, which corresponds to the pore diameter of the PAA template. The compactness of the nanotubes is quite high, about 1.0×10^9 cm^{-2}, corresponding to the pore density of the PAA. The energy-dispersive x-ray spectroscopies (EDSs) of the nanotubes shown in figure 1(c) confirmed that the nanotubes were composed of zinc and oxygen with the atomic ratio of about 1:1. The Au peak in figure 1(c) originates from the Au-sputtered sample for SEM measurement. The result indicates that the tubular ZnO nanostructures are highly pure, and there is no any contaminant of carbon, which could be attributed to the oxidation reaction with oxygen. X-ray diffraction (XRD) measurement was performed to probe the crystal structure and phase purity of the nanotubes. Figure 2 shows a typical XRD pattern of the ZnO nanotube arrays embedded in a PAA template. All diffraction peaks can be indexed as hexagonal wurtzite structure ZnO with lattice constants of $a = 3.25$ and $c = 5.20$ Å, which is consistent with the standard value for bulk hexagonal ZnO (JCPDS 36-1451). However, comparing the intensities of the (100) and (101) peaks of the nanotubes with those of the standard bulk hexagonal ZnO, it was found that the relative intensity of (100) peak has been dramatically improved, indicating that the nanoparticles composing nanotubes may have a different preferential growth direction from that of the bulk ZnO [19]. According to the Scherrer equation, the average sizes of the nanoparticles are about 16 nm.

The morphology and structure of individual ZnO nanotubes have been characterized in further detail using transmission electron microscopy (TEM) and selected-area electron diffraction (SAED). Figure 3(a) shows a typical TEM image of a single ZnO nanotube. It can be seen that the nanotube is straight and uniform along its whole length. The outer diameter and wall thickness of the nanotube are about 190 and 25 nm, respectively. The nanotube is composed of ZnO nanocrystals with sizes about 10–20 nm, which is consistent with above calculated value from the Scherrer equation. In addition, the corresponding SAED pattern (figure 3(b)) shows that the ZnO nanotubes are polycrystalline, and the diffraction rings observed in the SAED pattern can be indexed as the (100), (101), (102), (110), (103) and (112) lattice planes of hexagonal ZnO.

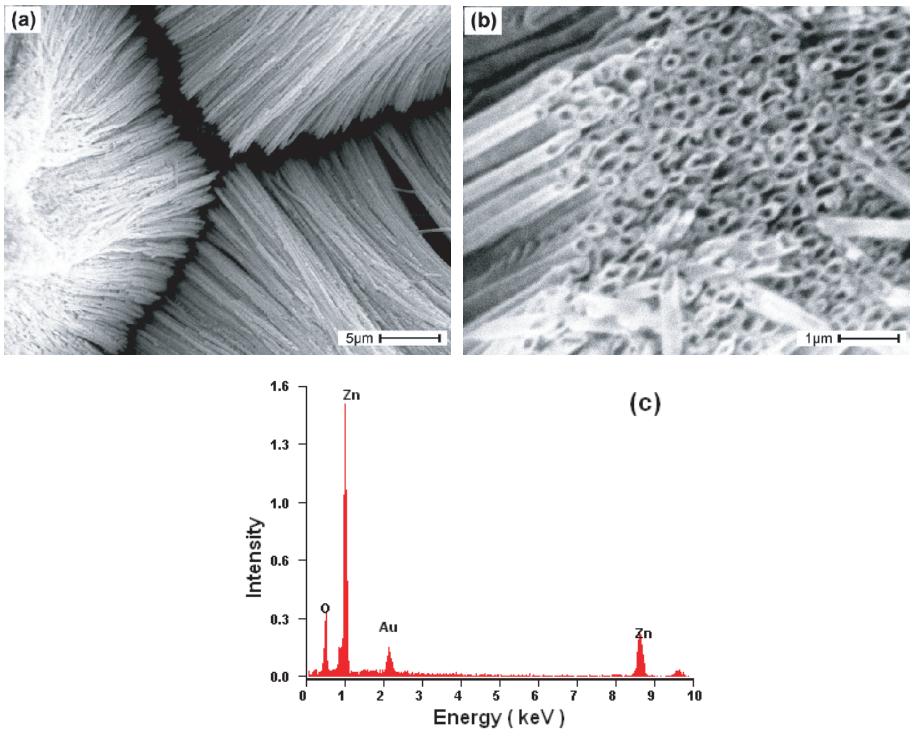

Figure 1. SEM images and an EDS spectrum of the as-prepared ZnO nanotubes. (a) Low-magnification image of aligned ZnO nanotubes. (b) Tilted view of ZnO nanotube arrays. (c) EDS spectrum of the nanotubes.
(This figure is in colour only in the electronic version)

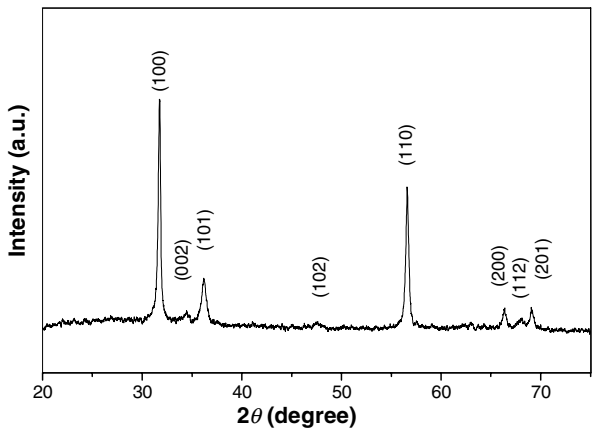

Figure 2. XRD pattern of the ZnO nanotube arrays embedded in PAA membrane.

The PL of the ZnO nanotubes with PAA support was measured at room temperature. Three emitting bands, including a strong violet band at 414 nm, a blue band at 462 nm, as well as a weak shoulder peak at around 480 nm, have been observed (figure 4). Since alumina has a band gap around 8.8 eV, the possibility that the observed PL was emitted from the coexisting alumina template could be excluded [23]. The PL of the ZnO nanotubes is considerably different from the typical observation in ZnO crystals, which usually exhibited a narrow UV peak at 370–390 nm and a broad green emission centred at 510–550 nm [24–26]. Recently, violet and blue luminescence such as 413 nm [27], ∼420 nm [28–31], 446 nm [32], ∼465 nm [20, 33] and ∼482 nm [29, 31] from ZnO thin film, nanoparticles, and whiskers have been reported. Violet emission at ∼413 nm observed in ZnO films has been attributed to the possible existence of cubic ZnO [27]. However, the emission centred at 414 nm in present sample could not originate from cubic ZnO due to the pure wurtzite phase of the nanotubular ZnO as shown in the XRD results. It can possibly be attributed to the interstitial oxygen and/or transition between defects (interface traps) at grain boundaries and the valence band, which have been proposed to explain the emissions at ∼420 nm [28–30]. The shoulder peak at 480 nm can be assigned to a transition between the oxygen vacancy and interstitial oxygen and/or lattice defects related to oxygen and zinc vacancies as reported previously [29, 31]. The blue band at 462 nm is similar to previously reported results for ZnO nanotubes (465 nm) [20] and ZnO nanorods (440–480 nm) [13], and may be in correlation with the defect structures. The quench of green luminescence might be ascribed to the low concentration of oxygen vacancies [34] in the ZnO nanotubes grown under oxygen-rich conditions. The quench of UV luminescence can be attributed to the poor crystalline quality of the ZnO nanotubes [29, 30].

Field emission properties of the ZnO nanotube array with an emitting surface area of 0.1 cm^2 are shown in figure 5. As can be seen from the J–E plot in figure 5, the turn-on threshold field is around 7.3 V μm^{-1} at a current density of 0.1 μA cm^{-2}. The field emission current density reaches 1.3 mA cm^{-2} at 11.8 V μm^{-1}, which is sufficient to excite the phosphor for flat panel display applications. These values are comparable

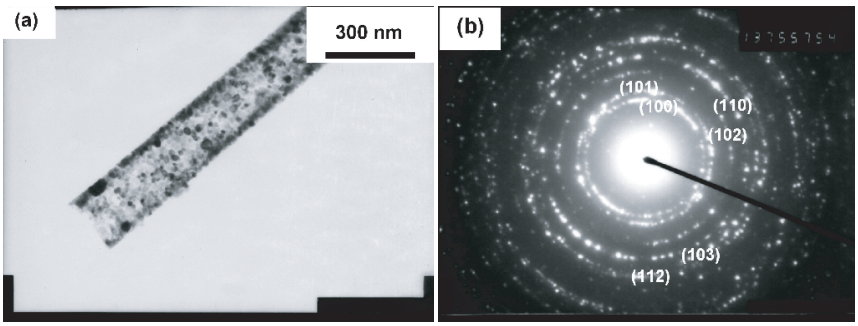

Figure 3. (a) TEM image and (b) SAED pattern of the ZnO nanotubes.

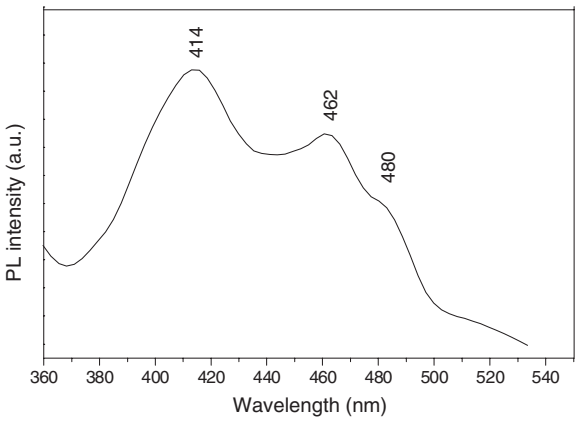

Figure 4. Room-temperature PL spectrum of the ZnO nanotubes embedded in PAA template under excitation at 302 nm.

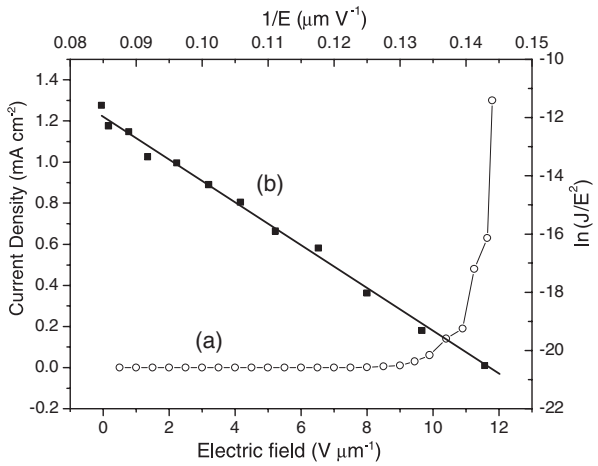

Figure 5. The dependence of the field emission current density J on the applied electric field strength E of the ZnO nanotube array. (a) J–E plot (○) and (b) Fowler–Nordheim relationship of $\ln(J/E^2)$–$1/E$ plot (■).

to those from a ZnO nanowire array obtained by Lee *et al* [8]. The exponential dependence between the emission current and the applied field, plotted in $\ln(J/E^2)$–$1/E$ relationship in figure 5, indicates that the field emission from ZnO nanotube array obeys the Fowler–Nordheim (FN) equation:

$$J = (A\beta^2 E^2/\phi)\exp(-B\phi^{3/2}/\beta E)$$

where J is the current density, E is the applied electric field, ϕ is the work function of the emitter material (5.3 eV for ZnO), A and B are constants with the value of 1.54×10^{-6} A eV V^{-2} and 6.83×10^3 V eV$^{-3/2}$ μm^{-1}, respectively, and β is the field enhancement factor at sharp geometry. The linear $\ln(J/E^2)$–$1/E$ plot indicates that the currents are field emission currents. From the slope of the $\ln(J/E^2)$–$1/E$ plot, the estimated field enhancement factor is 570, which is comparable to the reported results from ZnO nanowires [8], nanoneedles [16] and nanotips [35].

4. Conclusion

In summary, large-scale high-density and well-aligned ZnO nanotube arrays have been fabricated by a template-based CVD method. The ZnO nanotubes have diameters in the range 100–300 nm and lengths up to tens of micrometres. Compared with the template-based electrodeposition and vapour deposition methods, which all tend to form ZnO nanowires in the PAA membranes [6, 7], the present method possesses a unique advantage in fabricating ZnO nanotubes. The PL spectrum of the ZnO nanotube arrays at room temperature shows a strong violet emission at 414 nm, a blue band at 462 nm and a weak shoulder peak at around 480 nm. Field electron emission for ZnO nanotubes was studied for the first time. The turn-on electric field for the ZnO nanotube array was found to be about 7.3 V μm^{-1} at a current density of 0.1 μA cm^{-2}. The emission current density reached 1.3 mA cm^{-2} at a bias field of 11.8 V μm^{-1}. It is reasonable to expect that the ZnO/PAA assembly system fabricated by this approach can be applied to optoelectronic devices.

Acknowledgments

The authors are grateful for financial support from the National Natural Science Foundation of China (No. 20371026) and the University Natural Science Foundation of Jiangsu Province (04KJB150004).

References

[1] Dai L M, Patil A, Gong X Y, Guo Z X, Liu L Q, Liu Y and Zhu D B 2003 *Chem. Phys. Chem.* **4** 1150
[2] Rao C N R and Nath M 2003 *Dalton Trans.* 1

[3] Keis K, Vayssieres L, Lindquist S and Hagfeldt A 1999 *Nanostruct. Mater.* **12** 487
[4] Minne S C, Manalis S R and Quate C F 1995 *Appl. Phys. Lett.* **67** 3918
[5] Gorla C R, Emanetoglu N W, Liang S, Mayo W E, Lu Y, Wraback M and Shen H 1999 *J. Appl. Phys.* **85** 2595
[6] Liu C H, Zapien J A, Yao Y, Meng X M, Lee C S, Fan S S, Lifshitz Y and Lee S T 2003 *Adv. Mater.* **15** 838
[7] Zheng M J, Zhang L D, Li G H and Shen W Z 2002 *Chem. Phys. Lett.* **363** 123
[8] Lee C J, Lee T J, Lyu S C, Zhang Y, Ruh H and Lee H J 2002 *Appl. Phys. Lett.* **81** 3648
[9] Jo S H, Lao J Y, Ren Z F, Farrer R A, Baldacchini T and Fourkas J T 2003 *Appl. Phys. Lett.* **83** 4821
[10] Banerjee D, Jo S H and Ren Z F 2004 *Adv. Mater.* **16** 2028
[11] Zhang G, Zhang Q, Pei Y and Chen L 2004 *Vacuum* **77** 53
[12] Wang X, Summers C J and Wang Z L 2004 *Nano Lett.* **4** 423
[13] Wu J J and Liu S C 2002 *Adv. Mater.* **14** 215
[14] Yu K, Zhang Y, Xu R, Jiang D, Luo L, Li Q, Zhu Z and Lu W 2005 *Solid State Commun.* **133** 43
[15] Pan Z W, Dai Z R and Wang Z L 2001 *Science* **291** 1947
[16] Xu C X and Sun X W 2003 *Appl. Phys. Lett.* **83** 3806
[17] Tseng Y K, Huang C J, Cheng H M, Lin I N, Liu K S and Chen I C 2003 *Adv. Funct. Mater.* **13** 811
[18] Zhu Y W, Zhang H Z, Sun X C, Feng S Q, Xu J, Zhao Q, Xiang B, Wang R M and Yu D P 2003 *Appl. Phys. Lett.* **83** 144
[19] Zhang J, Sun L D, Liao C S and Yan C H 2002 *Chem. Commun.* 262
[20] Zhang X H, Xie S Y, Jiang Z Y, Zhang X, Tian Z Q, Xie Z X, Huang R B and Zheng L S 2003 *J. Phys. Chem.* B **107** 10114
[21] Hu J Q, Li Q, Meng X M, Lee C S and Lee S T 2003 *Chem. Mater.* **15** 305
[22] Yu H D, Zhang Z P, Han M Y, Hao X T and Zhu F R 2005 *J. Am. Chem. Soc.* **127** 2378
[23] French R H 1990 *J. Am. Ceram. Soc.* **73** 477
[24] Djurisic A B, Choy W C H, Roy V A L, Leung Y H, Kwong C Y, Cheah K W, Gundu Rao T K, Chan W K, Lui H F and Surya C 2004 *Adv. Funct. Mater.* **14** 856
[25] Egelhaaf H J and Oelkrug D 1996 *J. Cryst. Growth* **161** 190
[26] Bethke S, Pan H and Wessels B W 1998 *Appl. Phys. Lett.* **52** 138
[27] Sekiguchi T, Haga K and Inaba K 2000 *J. Cryst. Growth* **214/215** 68
[28] Xu X L, Lau S P, Chen J S, Chen G Y and Tay B K 2001 *J. Cryst. Growth* **223** 201
[29] Mahamuni S, Borgohain K, Bendre B S, Leppert V J and Risbud S H 1999 *J. Appl. Phys.* **85** 2861
[30] Jin B J, Im S and Lee S Y 2000 *Thin Solid Films* **366** 107
[31] Hu J Q, Ma X L, Xie Z Y, Wong N B, Lee C S and Lee S T 2001 *Chem. Phys. Lett.* **344** 97
[32] Xue Z Y, Zhang D H, Wang Q P and Wang J H 2002 *Appl. Surf. Sci.* **195** 126
[33] Dai L, Chen X L, Wang W J, Zhou T and Hu B Q 2003 *J. Phys.: Condens. Matter* **15** 2221
[34] Vanheusden K, Warren W L, Seager C H, Tallant D K, Voigt J A and Gnade B E 1996 *J. Appl. Phys.* **79** 7983
[35] Hung C H and Whang W T 2004 *J. Cryst. Growth* **268** 242